Adsorption and Inactivation of SARS-CoV-2 on the surface of anatase TiO_2(101)

Mona Kohantorabi,[*,†] Michael Wagstaffe,[†] Marcus Creutzburg,[†] Aldo Ugolotti,[‡] Satishkumar Kulkarni,[†] Arno Jeromin,[†] Tobias Krekeler,[¶] Martin Feuerherd,[§,‖] Alexander Herrmann,[⊥] Gregor Ebert,[§] Ulrike Protzer,[§] Gabriela Guédez,[#] Christian Löw,[#] Roland Thuenauer,[@,△] Christoph Schlueter,[▽] Andrei Hloskovsky,[▽] Thomas F. Keller,[†,††] Cristiana Di Valentin,[‡] Andreas Stierle,[†,††] and Heshmat Noei[*,†]

†*Centre for X-ray and Nano Science (CXNS), Deutsches Elektronen-Synchrotron (DESY), 22607 Hamburg, Germany*

‡*Dipartimento di Scienza dei Materiali, Università degli Studi di Milano-Bicocca, Via Cozzi 55, 20125 Milano, Italy*

¶*Electron Microscopy Unit, Hamburg University of Technology, Eissendorfer Strasse 42, 21073, Hamburg, Germany*

§*Institute of Virology, Technical University of Munich/Helmholtz Munich, Munich, Germany*

‖*Division of Gastroenterology, Massachusetts General Hospital and Harvard Medical School, Boston, USA*

⊥*Institute of Virology, Helmholtz Munich, Ingolstädter Landstraße 1, 85764, Neuherberg, Germany*

#*Centre for Structural Systems Biology (CSSB), Deutsches Elektronen-Synchrotron (DESY), EMBL Hamburg, 22607 Hamburg, Germany*

@*Technology Platform Light Microscopy and Image Analysis (TP MIA), Leibniz Institute for Experimental Virology (HPI), Hamburg, Germany*

△*Centre for Structural Systems Biology (CSSB), Hamburg, Germany*

▽*Deutsches Elektronen-Synchrotron (DESY), 22607 Hamburg, Germany*

††*Department of Physics, University of Hamburg, Notkestraße 9-11, 22607 Hamburg, Germany*

E-mail: mona.kohantorabi@desy.de; heshmat.noei@desy.de

Abstract

We investigated the adsorption of severe acute respiratory syndrome corona virus 2 (SARS-CoV-2), the virus responsible for the current pandemic, on the surface of the model catalyst TiO_2(101) using atomic force microscopy, transmission electron microscopy, fluorescence microscopy and X-ray photoelectron spectroscopy, accompanied by density functional theory calculations. Three different methods were employed to inactivate the virus after it was loaded on the surface of TiO_2(101): i) ethanol, ii) thermal and iii) UV treatments . Microscopic studies demonstrate that the denatured spike proteins and other proteins in the virus structure readsorb on the surface of TiO_2 under thermal and UV treatments. The interaction of the virus with the surface of TiO_2 was different for the thermally and UV treated samples compared to the sample inactivated via ethanol treatment. AFM and TEM results on the UV-treated sample suggested that the adsorbed viral particles undergo damage and photocatalytic oxidation at the surface of TiO_2(101) which can affect the structural proteins of SARS-CoV-2 and denature the spike proteins in 30 minutes. The role of Pd nanoparticles (NPs) was investigated in the interaction between SARS-CoV-2 and TiO_2(101). The presence of Pd NPs enhanced the adsorption of the virus due to the possible interaction of the spike protein with the NPs. This study is the first investigation of the interaction of SARS-CoV-2 with the surface of single crystalline TiO_2(101) as a potential candidate for virus deactivation applications. Clarification of the interaction of the virus with the surface of semiconductor oxides will aid in obtaining a deeper understanding of the chemical processes involved in photo-inactivation of microorganisms, which is important for the design of effective photocatalysts for air purification and self-cleaning materials.

Introduction

In late 2019, the Corona virus disease (COVID-19) caused by the severe acute respiratory syndrome corona virus 2 (SARS-CoV-2) led to a global pandemic.[1] SARS-CoV-2, with a spherical shape and a size of around 80-120 nm,[2] has four important structural proteins

namely spike (S), membrane (M), envelope (E), and nucleocapsid (N) proteins and some non-structural proteins that can adjust the cellular responses[3](Figure 1). S-protein, with a club-like shape of 20 nm in length, is the outermost structure in SARS-CoV-2 and is responsible for the entrance of the virus into the cell.[4–6] SARS-CoV-2 can be transmitted through droplets produced by the infected person, by direct contact, via contaminated surfaces and by the inhalation of small respiratory droplets and aerosol particles.[7] It has been reported that SARS-CoV-2 can survive more than three hours in aerosols[8] and is stable on stainless-steel surfaces and plastic with a half-life of approximately 5.6 and 6.8 hours, respectively.[9] Moreover, Ong et al. reported that the RNA of SARS-CoV-2 was observed in air.[10] Owing to the role of air and surface contamination in SARS-CoV-2 transmission, the development of self-decontaminating materials with low cytotoxicity should be considered. Recently, various treatment methods have been reported for the inactivation of viruses such as chemical disinfection with alcohol,[11] formaldehyde,[12] peroxide,[13] hypochlorous acids[14] and mechanical sterilization using ultraviolet (UV) light irradiation[15] and heating.[16] Disinfection methods can affect the lipid bilayer and denature the spike proteins during the early stages of virus deactivation.[17,18] Due to the high surface stability of SARS-CoV-2 that enhances the efficiency of virus transmission,[17] cost effective and efficient methods are required for virus inactivation on surfaces.

Solid state antiviral materials are preferable to solvent-based ones due to their improved robustness and long term stability.[19] Oxide nanomaterials are promising candidates for the removal and inactivation of viral/bacterial infections as well as for preventing pathogen dissemination.[20,21] Titanium dioxide (TiO_2), with unique properties such as low toxicity, high photoactivity and high commercial availability compared to other semiconductors,[22,23] has received considerable attention for environmental applications such as solid-state antiviral materials, self-cleaning surfaces and air and water purification systems.[24,25] Multiple competing reaction pathways can be responsible for virus inactivation over nanomaterials, such as catalytic oxidation, metal ion release, photo-thermal effects, and formation of reactive

oxygen species (ROS).[26] Among different advanced oxidation processes, which are used for the elimination of organic and inorganic pollutants and inactivation of microorganisms, photocatalysis is the most desirable method owing to the high ability in inactivation of different types of contaminants.[27] By passing the polluted air over a photocatalyst, pollutants can adsorb on the photocatalyst surface and can be converted to harmless and low toxic compounds via the formation of holes (h^+) with high oxidation potential[19] and ROS such as superoxide radical ($^{\bullet}O_2^-$), hydroxyl radical ($^{\bullet}OH$) and H_2O_2 under light irradiation.[28–30] Consequently, photocatalyst surfaces can facilitate virus disinfection, mineralize the organic compounds in the virus structure[31] and inhibit the spread of the virus via the contaminated surfaces.[32,33] Different methods such as the combination of noble metal and metal oxides have been reported to improve the photocatalytic activity of TiO_2 for the inactivation of SARS-CoV-2 in solution.[19,34] Nanoparticles (NPs) with a small size and high surface to volume ratio show high adsorption capacity for amino acids and peptides.[35] It was shown that gold (Au) and silver (Ag) NPs interact with peptide and human immunodeficiency virus 1 (HIV-1), respectively.[36,37] NPs can bind to the viral genome and modulate the viral transcription.[38] Recently, it was reported that SARS-CoV-2 can adsorb on metal surfaces such as Au NPs,[39] oxygen-containing substrates (e.g. glass, paper, wood),[40] and surface hydroxyl groups.[41] Depending on the surface functional groups, active sites and surface humidity, the adsorption capacity of SARS-CoV-2 can be influenced.[41] The functional groups of amino acids in S-proteins of virus, play a vital role in the adhesion process. Recently, the photoactivity of Ag-TiO_2 single atom nanozyme,[42] Ag NPs@TiO_2,[34] Cu_xO/TiO_2[43] and TiO_2/Ti–O on Al_2O_3 balls[44] have been investigated for the removal and inactivation of SARS-CoV-2. The studies were performed in aqueous solution and only the reaction solution was tested to identify the virus inactivation applying catalysts. In fact, most of the data surrounding microorganism inactivation, especially virus inactivation, is reported in the liquid phase[34,42,43] and there is limited knowledge about the adsorption of SARS-CoV-2 on the surface of catalysts or at the interface between the virus and the catalyst. Therefore, obtaining more detailed information

regarding the adsorption/inactivation behavior of SARS-CoV-2 at the surface and interface of TiO_2 as well as the role of NPs can lead to the development of efficient antiviral coatings and aid in the design of advanced materials for the photocatalytic inactivation of viruses. In this study, we investigated the adsorption of SARS-CoV-2 on single crystalline $TiO_2(101)$, the thermodynamically most stable facet of anatase,[45] and on $TiO_2(101)$ supported Pd NPs. Thermal and ethanol treatments were employed to inactivate the SARS-CoV-2 particles adsorbed on the surface of $TiO_2(101)$. Moreover, the UV induced photo-inactivation of SARS-CoV-2 adsorbed on $TiO_2(101)$ was investigated. These methods were employed before the samples were transferred out of the biosafety level (BSL)-3 laboratory. We characterized the samples using atomic force microscopy (AFM), transmission electron microscopy (TEM), scanning tunneling microscopy (STM), fluorescence microscopy (FM) and X-ray photoelectron spectroscopy (XPS), combined with density functional theory (DFT) calculations. The main objective of our present work is to identify the adsorption and inactivation behavior of SARS-CoV-2 on the surface of the model photocatalyst $TiO_2(101)$.

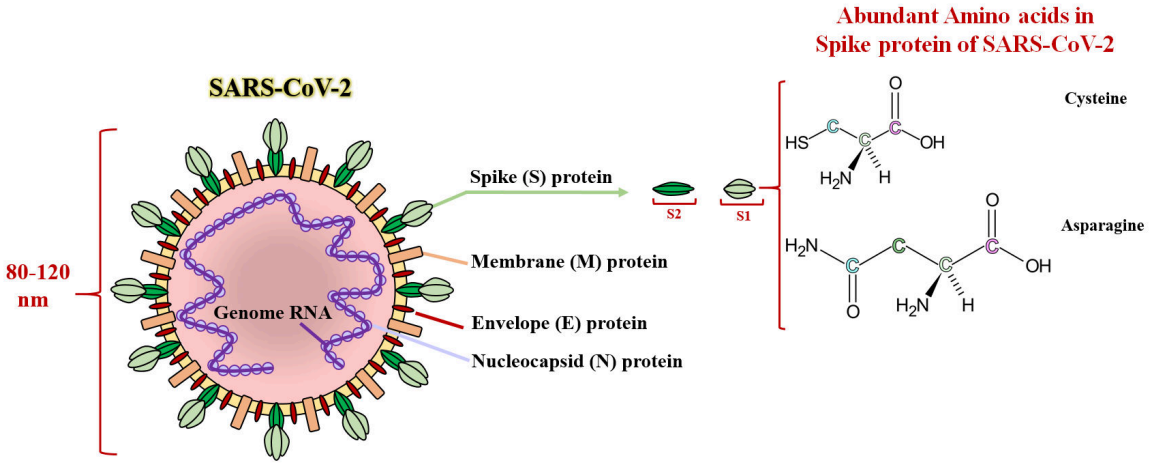

Figure 1: Schematic structure of SARS-CoV-2.

Results and discussion

Characterization of Cell Culture Media (CCM) on TiO_2(101)

As described in the methods section, SARS-CoV-2 suspension contains CCM. To obtain more information about the CCM structure, as well as to distinguish it from the virus particles, atomic force microscopy was employed to study the CCM on the surface of TiO_2(101). According to the AFM images (Figure 2 a and b), no particle structure was observed. CCM forms a fiber-like structure on the surface of TiO_2(101) with a thickness of around 14-45 nm (Figure 2 c).

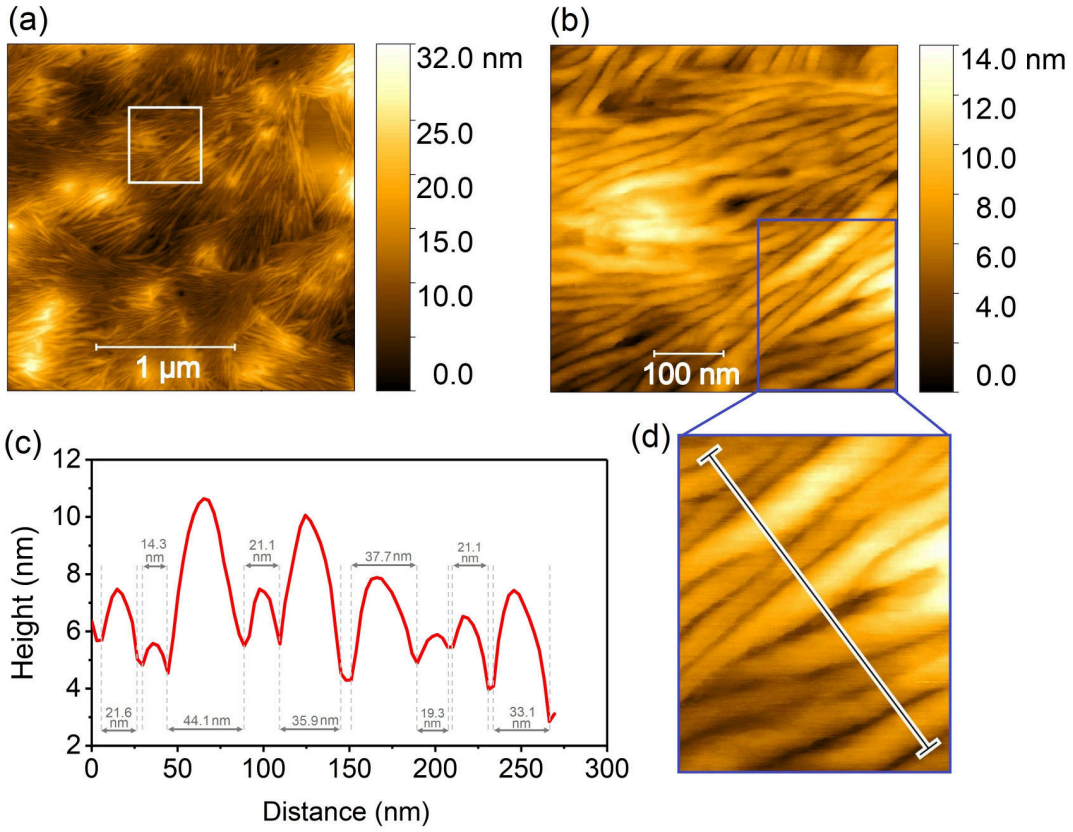

Figure 2: (a) AFM (2.5× 2.5 μm^2) image of CCM adsorbed on the surface of TiO_2(101) after thermal treatment at 70 °C. (b) AFM image (0.5 × 0.5 μm^2) of marked area with white rectangle in image (a). (c) Line scan profile from top to down in zoomed area (d) of image (b).

Adsorption of SARS-CoV-2 on the surface of TiO_2(101)

To further confirm the adsorption of SARS-CoV-2 on TiO_2(101), fluorescence microscopy was applied. Anatase TiO_2(101) coated with CCM was measured as a reference sample. Rabbit anti-SARS-CoV-2 nucleocapsid primary antibodies and anti-rabbit secondary antibodies conjugated to Alexa568 were used to fluorescently label the virus particles in the samples by indirect immunofluorescence. Mean fluorescence intensities for SARS-CoV-2 and CCM on TiO_2(101) were obtained to be 6160 and 2902, respectively. The comparatively high fluorescence intensity of the virus sample confirms the adsorption of SARS-CoV-2 on the surface of TiO_2. Compared to the virus sample, only faint green signal was detected for CCM on TiO_2(101) (see Figure S1 in the supporting information) attributed to autofluorescent proteins and other components in CCM.

Comparing the various inactivation methods of SARS-CoV-2 adsorbed on the surface of TiO_2(101)

Inactivation of the Corona virus was necessary for the transfer of materials from the biosafety level (BSL)-3 laboratory to other laboratories allowing for accelerated studies against SARS-CoV-2 during the pandemic.[13] Recently, Lyonnais et al. reported a new inactivation method in solution media that kept the virus particles intact but inactivated.[12] They found that under heating treatment (58 °C for 30 min) in solution media, the virus molecules lost their spherical structure and became damaged, while upon formaldehyde (FA) treatment SARS-CoV-2 was inactivated but the structure remained intact.[12] In this study, thermal inactivation was done by incubating the sample at 70 °C for 30 min after loading the SARS-CoV-2 on the surface of TiO_2(101) (see Methods section) and then the sample was analyzed by AFM and TEM. Although this inactivation method denatures the proteins, it still allows one to obtain information about the adsorption behavior of SARS-CoV-2 at the surface of TiO_2(101). Based on the AFM images shown in Figure 3 a and b (i), several small and large

particles were observed for SARS-CoV-2 adsorbed on TiO_2(101) following thermal inactivation, while no particles were detected in CCM on the surface of TiO_2 (Figure 2). Therefore, these particles come from the virus structure. According to the AFM images for ethanol and thermal treatments (Figure 3), the observed spherical particles with the particle diameter in the range of 75-100 nm correspond to the virus structure. However the height of the particles in these images is smaller than the expected virus diameter (80-120 nm). Due to drying of the sample, viruses become flatter on the surface of TiO_2(101). Based on the line scan profiles (Figure 3a and b (ii)), the heights of adsorbed SARS-CoV-2 on TiO_2 are 19.6 nm and 9-10 nm under ethanol and thermal treatments, respectively. It is known that temperature can affect the structure of biomacromolecules such as protein, lipids and nucleic acids.[46,47] Since the thermal treatment was performed before the AFM measurement, the virus proteins and membrane could have denatured and adsorbed on the surface of TiO_2. Contrary to ethanol treatment, the area surrounding the virus is covered by the cell by-products layer, which have a smaller size than SARS-CoV-2 (Figure 3 b(ii)). In fact, after ethanol treatment most of the adsorbed virus particles were removed from the catalyst surface via the surface washing. Lipid bilayer envelope in SARS-CoV-2 contains the S, E, and M proteins.[40] The virus can be inactivated by disruption of the lipid envelope. Under ethanol treatment, ethanol dissolves this layer that leads to the inactivation of the virus.[48]

Under ethanol and thermal treatments, AFM images could not show the S-protein on the virus structure. Due to the virus movements on the surface of TiO_2(101) during the adsorption, and the subsequent inactivation methods, the S-proteins may break. We are not able to directly monitor the mechanism of the interaction of the virus with the surface of the catalyst and their subsequent self-assembly, as they could not be delivered out of the BSL-3 laboratory. However, for the first time we have clear evidence that the virus interacts with the surface and that the conditions at the interface play an instrumental role in the mechanism of adsorption and denaturation of the virus.

Recently, Rath and Kumar reported that the spike protein conformation depends on tem-

perature.[47] At temperatures exceeding 50 °C, the receptor binding motif (RBM) in the spike protein structure is completely closed, resulting in the inactivation of SARS-CoV-2. Clearly, ethanol washes the virus away, and therefore there are less virus particles on the surface of TiO_2(101), while through thermal treatment the adsorbed viruses are dried on the surface of TiO_2 and therefore more proteins are dissociated from the virus structure after thermal treatment. Denatured S-proteins and other virus proteins (from the virus envelope and membrane) dissociate and adsorb at the surface of TiO_2(101). Figure 3 a and b (iii) show the TEM images of SARS-CoV-2 adsorbed on TiO_2(101) that was initially inactivated by ethanol and thermal treatments, respectively. Spherical particles with a size of around 110 nm correspond to SARS-CoV-2. As we expected, compared to ethanol treatment, small particles in the diameter range of 10-45 nm were observed in the TEM image of the thermally treated sample (see the labeled region with a yellow rectangle in Figure 3 b (iii)). These results are in good agreement with the AFM images shown in Figure 3 a and b, confirming the effect of heat on the virus structure and its inactivation.

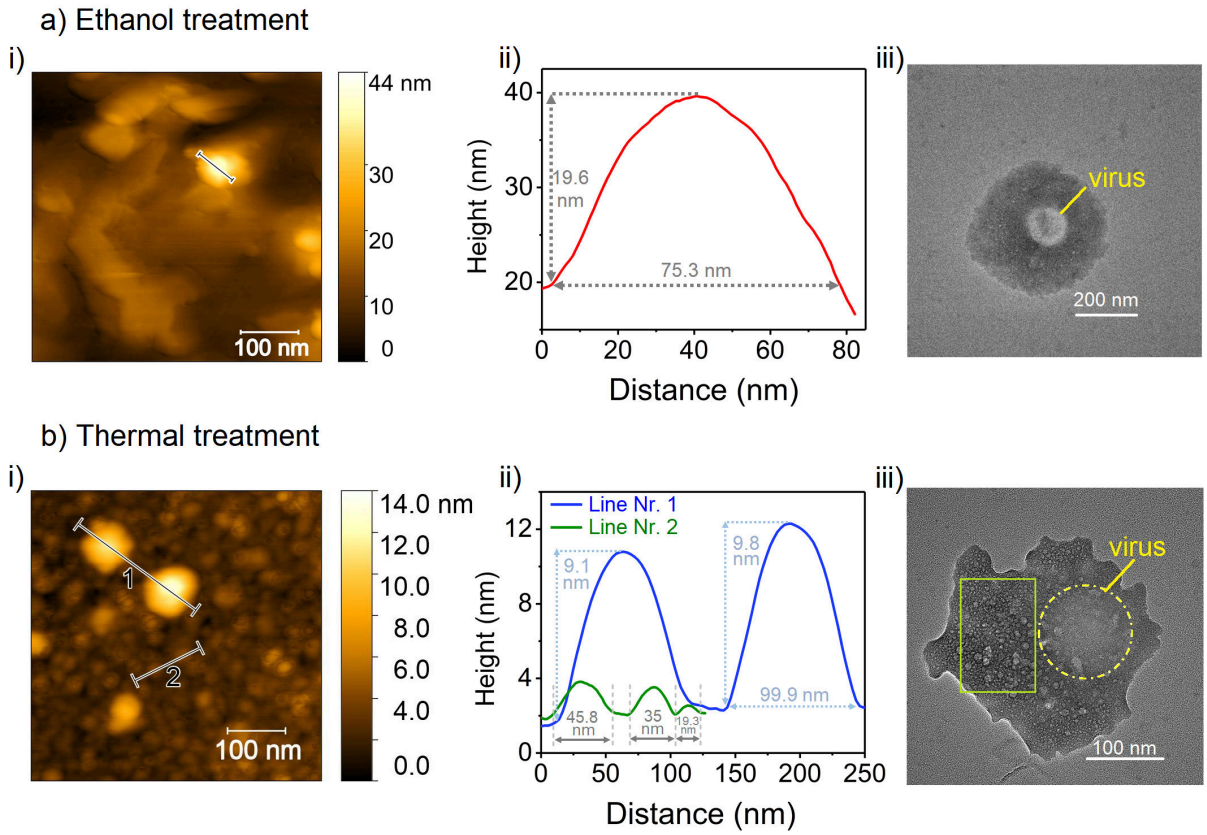

Figure 3: AFM ($0.5 \times 0.5\ \mu m^2$) images of SARS-CoV-2 adsorbed on $TiO_2(101)$ (i), line scan profile measured along the particles in AFM images (black lines) (ii) and TEM images (iii) of SARS-CoV-2 adsorbed on $TiO_2(101)$ after ethanol (a) and thermal (b) treatments.

X-ray photoelectron spectroscopy (XPS) analysis of adsorbed cell culture media (CCM) and inactivated SARS-CoV-2 on the surface of $TiO_2(101)$

To obtain more information on the chemical composition of the system and to further prove the adsorption and interaction of the virus with the surface of $TiO_2(101)$ as well as the role of different functional groups on virus adsorption, we performed XPS experiments. To better distinguish the adsorbed virus from CCM using the XPS results, the adsorbed CCM on $TiO_2(101)$ before and after thermal treatment were also measured. We also studied the interaction of the denaturated peptide chain of the spike protein theoretically through simplified models involving single amino acids, i.e. cysteine (cys) or asparagine (asn), onto the anatase $TiO_2(101)$ surface, whose optimized structures and adsorption energies are reported

in Figure 4. Then, for each of these models, we calculated the C 1s binding energies.

Our aim is not to determine the most stable adsorption configuration of the amino acids, but it is to conceive configurations that resemble cysteine or asparagine as a part of a long peptide chain and understanding their interactions with the surface. This goal requires that either both or at least one of the amino acid groups involved in the peptide bonds of the actual primary chain (amino on one side and carboxylic on the other) are only weakly interacting with the surface. In the case of cysteine, we considered the carboxyl, the amino and the thiol as adsorbing groups: our results suggest that covalent, electrostatic and hydrogen bond interactions take place. The first model (Figure 4 b) is an exception with respect to this requirement, because both the amino and the carboxylic groups are interacting strongly with the surface, whereas the side chain of the amino acid containing the thiol (–SH) group is not. This configuration has been computed for comparison with a similar adsorption model, which has been previously reported in literature as the most favored configuration for cys/TiO_2(101).[49]

In this work, we find that it is not as stable as another configuration (Figure 4 d), where the thiol and the amino groups are coordinated to two surface Ti atoms and the OH of the carboxylic group establishes a hydrogen bond with a surface O atom. We should note here that the de-protonation of the thiol group is found to be unfavorable and has not been reported. Also, the zwitterionic form of the amino acid on the surface was only found in the model in Figure 4 b, where, the proton is transferred from the amino group to a surface O atom. We expect that the presence of water in the simulations would further stabilize the zwitterionic form, as suggested by several studies.[49–51] In the case of asparagine, we limited the study to one configuration, where only the side chain is involved in the interaction with the surface, except for a H-bond of the carboxylic OH, again with the aim of representing asparagine as part of a virtual peptide chain.

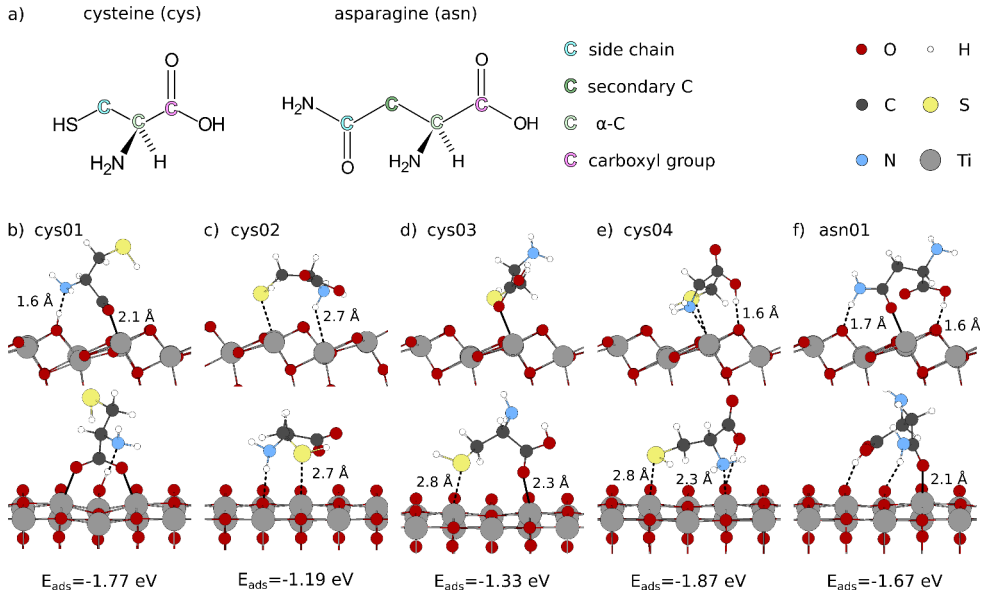

Figure 4: (a) Chemical structure of cysteine and asparagine in the neutral form, along with the chemical labeling of C atoms. (b)-(f) Left (upper row) and front (lower row) views of the optimized models of cys or asn adsorbed on anatase TiO_2(101) surface. In each panel, the adsorption energy (E_{ads}=$E_{cys,asn/TiO_2}$-$E_{cys,asn}$-E_{TiO_2}) and the most relevant distances are reported. The color code of the atom is reported in the top corner of the image. The solid/dashed black lines mark covalent bonds/electrostatic or H-bond interactions.

Experimentally, we focused on the core-level spectra for the Ti 2p, C 1s, O 1s, and N 1s for the as-prepared surface of TiO_2 (i), the same surface following the deposition of CCM (ii) and subsequent thermal treatment (iii), and inactivated SARS-CoV-2 on TiO_2 after heating to 70 °C (iv) (Figure 5). Regarding the experimental Ti 2p core level spectra shown in Figure 5 a, two dominant peaks were observed at binding energies (BEs) 458.3 and 464.1 eV that correspond to the Ti $2p_{3/2}$ and Ti $2p_{1/2}$ spin-orbit split components Ti^{4+} in TiO_2(101).[52] The small peaks located at 457.2 and 462.8 eV belong to the Ti $2p_{3/2}$ and Ti $2p_{1/2}$ components, attributed to small amounts of Ti^{3+}.[53] The C 1s core level for CCM can be fitted with five components at BEs of 283.6 eV (C=C),[54] 284.95 eV (C–H),[55] 286.5 eV (C–N and C=N,[56] C–OH,[57] C–SH[58]), 287.9 eV (C=O and O=C–N), and 289.4 eV (O=C–O).[54] Compared to CCM, the ratio of observed peaks at 284.95 eV and 286.5 eV was greater for the virus containing sample. As it was expected, this is due to the hydrocarbon groups present as side chains in the protein structure and this is greater in the virus adsorbed sample due to

a higher number of proteins and lipids. Figure 6a shows the difference spectrum of C 1s obtained by subtracting the C 1s spectrum of the virus from CCM. Based on this result, the contribution of virus in the C 1s spectrum was obtained. The dominant contribution was related to the C–H and C=O in the virus protein structure.

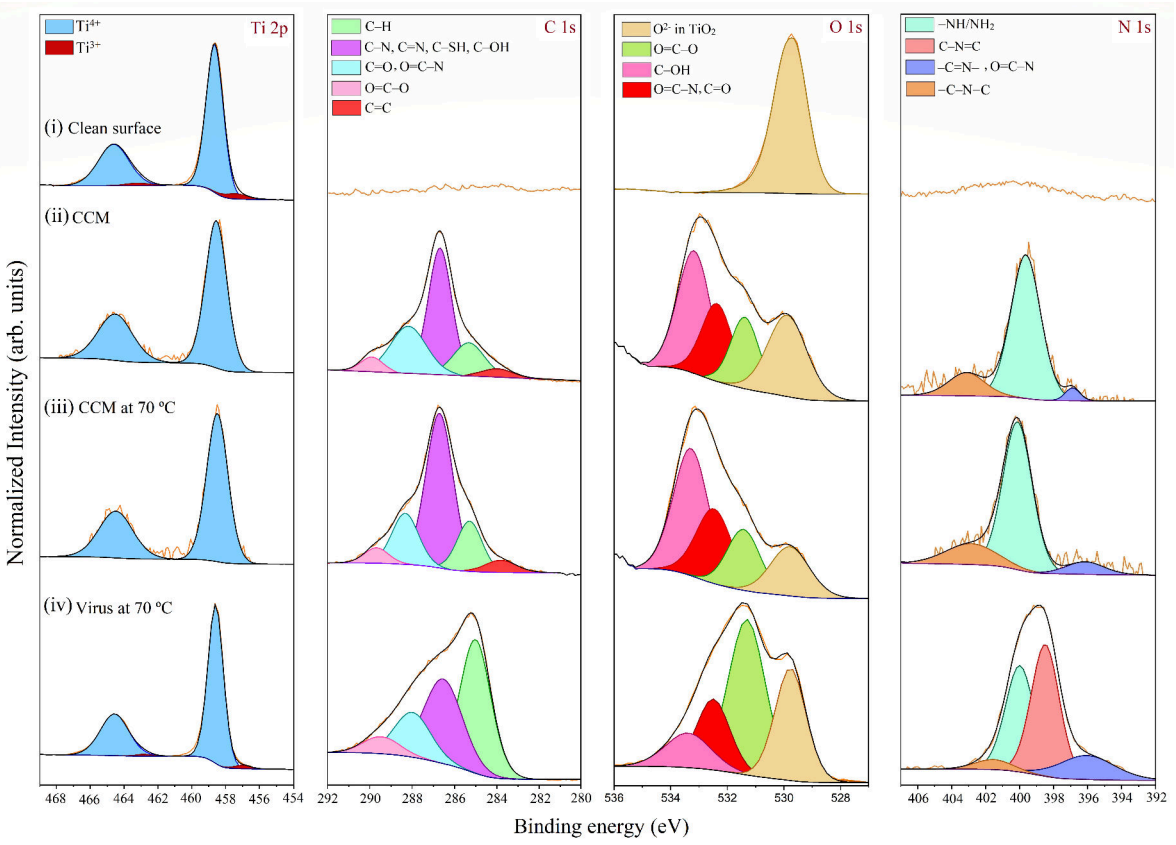

Figure 5: Core-level photoelectron spectra of Ti 2p (a), C 1s (b), O 1s (c), and N 1s (d) for clean surface of TiO_2(101) (i), adsorbed CCM before (ii) and after (iii) thermal treatment, and adsorbed SARS-CoV-2 after heating at 70 °C (iv). SARS-CoV-2 adsorbed on TiO_2(101) was measured at P22 beamline with a photon energy of 3.4 keV, while measurements for the adsorbed CCM before and after thermal treatment were performed at a photon energy 1.4 keV.

The actual interaction of the virus with the surface can be confirmed by the C 1s simulated results, shown in Figure 6 b-e, where three broad components can be resolved, matching the experimental ones (represented by green, magenta and cyano sticks, respectively). The two features at higher binding energy (BE) are shifted by $\sim$ 1.5 and 2.8 eV with respect to the secondary C (Figure 4 a) in the side chain of asn (that is computed to be the least bound), against an experimental shift of 1.55 and 2.95 eV. The peak at the lowest BE, besides the secondary C atoms (C–H), includes also the Cα of both cys (for all configurations considered) and asn. This would provide a rationalization for the high intensity of such peak, as observed in the experimental XPS (see Table 1 in the supporting information (S2)). At intermediate BEs, our models suggest the contribution of the C atoms in the carboxylic group, which is however strongly dependent on the adsorption configuration. This agrees with the broad experimental feature at 286.5 eV. Finally, at the highest BEs we register the contribution of the C atoms in the side chains of the amino acids, either the C bound to the thiol for cys or the C in the amide group for asn. The position of this third feature is in worse agreement with experiments, which is probably due to the contribution of other amino acids in the spike protein not considered in the computational model.

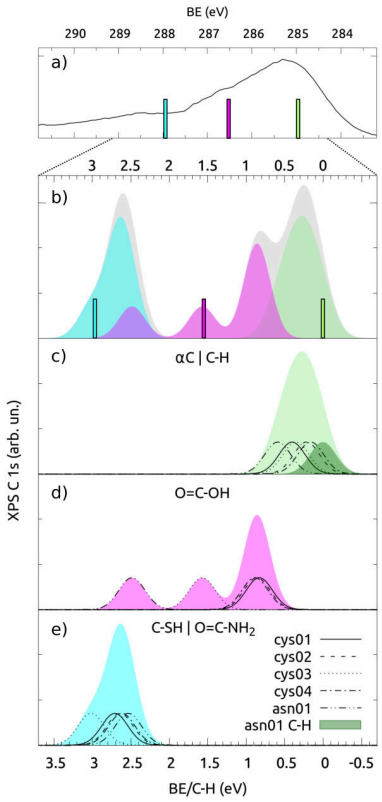

Figure 6: (a) Experimental C 1s XPS spectrum of the virus only, after CCM subtraction. The vertical sticks report the position of the fitted components shown in Figure 5 b, using the same color code. (b) Simulated C 1s XPS spectrum obtained as the overlap of all C species in all models. The simulated spectrum is aligned with the experimental one by matching the position of the component with the lowest BE to that of the fitted C-H feature and the dotted lines highlight the zoom in the energy range. (b), (c) and (d) report the separated contributions along with the individual components originated by inequivalent C atoms in various models considered. The BEs are reported with respect to the calculated energy of the secondary C in asn (C–H).

The O 1s core level peak of CCM was de-convoluted into four peaks (Figure 5 c). These peaks were observed at BEs 529.8 eV, 531.4 eV, 532.3, and 533.1 eV, which are assigned to the lattice oxygen in TiO_2, O=C–O, C=O/O=C–N (peptide or amide bond) and C–OH species, respectively.[57,59] All these peaks were also observed in the O 1s core level spectrum of the virus and CCM samples after thermal treatment. The changes observed in the peaks ratio in O 1s spectrum of the virus sample after thermal treatment are related to the presence of proteins and lipid structures in the virus. The N 1s core level spectrum after adsorption of CCM (Figure 5 d) can be fit with three components at binding energies of 396.8 eV, 399.6

eV, and 402.7 eV that correspond to the imine group (–C=N– and O=C–N),[60] –NH_2/–NH and –C–N–C,[61] respectively. Due to the presence of glutamine and non-essential amino acids in CCM, the amine and imine components were observed in the N 1s spectrum of CCM. In addition, dulbecco's modified eagle's medium (DMEM) in CCM contains four fold concentrations of amino acids and vitamins. Some of these vitamins contains imine group for which the corresponding peak was observed in the N 1s spectra. After thermal treatment, the –C=N– peak was slightly changed and broadened which could be related to the reaction between amino acids and carbonyl groups resulting in formation of imines through elimination of H_2O under thermal treatment. Similar behavior was detected for the –C=N– peak in the virus sample. In fact under thermal treatment, denatured proteins lose their 3D structure and can show conformational changes. Moreover, through inter-chain cross linking between –NH_2 and –COOH groups in the virus proteins new compounds can be formed, which can change the C 1s, O 1s and N 1s peak ratios and shape of virus sample compared to the CCM.

Photocatalytic inactivation of SARS-CoV-2 adsorbed on the surface of TiO_2(101)

UV (200-280 nm) irradiation is a potentially effective disinfection method that is widely used for disinfection of surfaces and is able to deactivate different types of viruses including SARS-CoV-2.[62] Under UV irradiation, RNA absorbs the UV photon which blocks the transcription via the formation of pyrimidine dimers, while absorption of UV radiation by amino acids disturbs the activity and structural function of the proteins.[63] However, the disinfection mechanism of SARS-CoV-2 under UV irradiation is not clear and requires further investigation. Recently, Lo et al.[64] reported the effect of UV-C (253.7 nm) irradiation on inactivation of SARS-CoV-2 in the liquid phase. TEM and protein damage testing results revealed that UV-C can deactivate the virus particles while their viral morphology remains intact.[64] Immunoblotting results of viral S- and N-proteins confirmed that protein degradation might not be the main reason for the UV-induced inactivation of the virus.[64] UV light with wavelengths ranging from 220-280 nm can damage the viral genome since this wavelength is close to the absorption wavelength of the virus nucleic acid.[65]

To study the effect of UV light on the virus adsorbed on the surface of TiO_2(101), the sample was exposed to UV light for 30 min (with a fixed distance between the sample and UV lamp of 10 cm) and then characterized by AFM and TEM out of the BSL-3 laboratory.[66] A Plaque assay test was performed in order to investigate the number of infectious viruses present after UV treatment. Contrary to the dark condition, where the virus particles remained active, complete virus inactivation was achieved after 30 min of UV irradiation.

The AFM images of the UV-treated samples (Figure 7 a) shows spherical particles with a size of around 80-120 nm (shown in the line profile in Figure 7 b) corresponding to the adsorbed SARS-CoV-2 particles on the surface of TiO_2(101). Some particles did not change in size and are intact with spike, confirming that one of the inactivation mechanisms under UV irradiation could be RNA damage without an obvious effect on viral structural proteins. Other particles with smaller size (20-30 nm) are related to the viral proteins membrane which dissociated from the virus structure under UV light and readsorbed on the surface of

TiO_2(101) (Figure 7 a, b). Figure 7 c displays the TEM images of SARS-CoV-2 adsorbed on the surface of TiO_2(101) after UV treatment. These results reveal that the virus morphology changed after UV treatment and the virus diameter was enlarged in line with the AFM results (see the labeled region with a yellow rectangle in Figure 7 a). In addition, surface S-proteins were not detected in the TEM results which confirmed that virus particles lost S-proteins following adsorption on the surface of TiO_2 and subsequent UV inactivation. Our results suggest that, the TiO_2(101)/UV photocatalytic system inactivated SARS-CoV-2 by viral genome damage and viral proteins degradation.

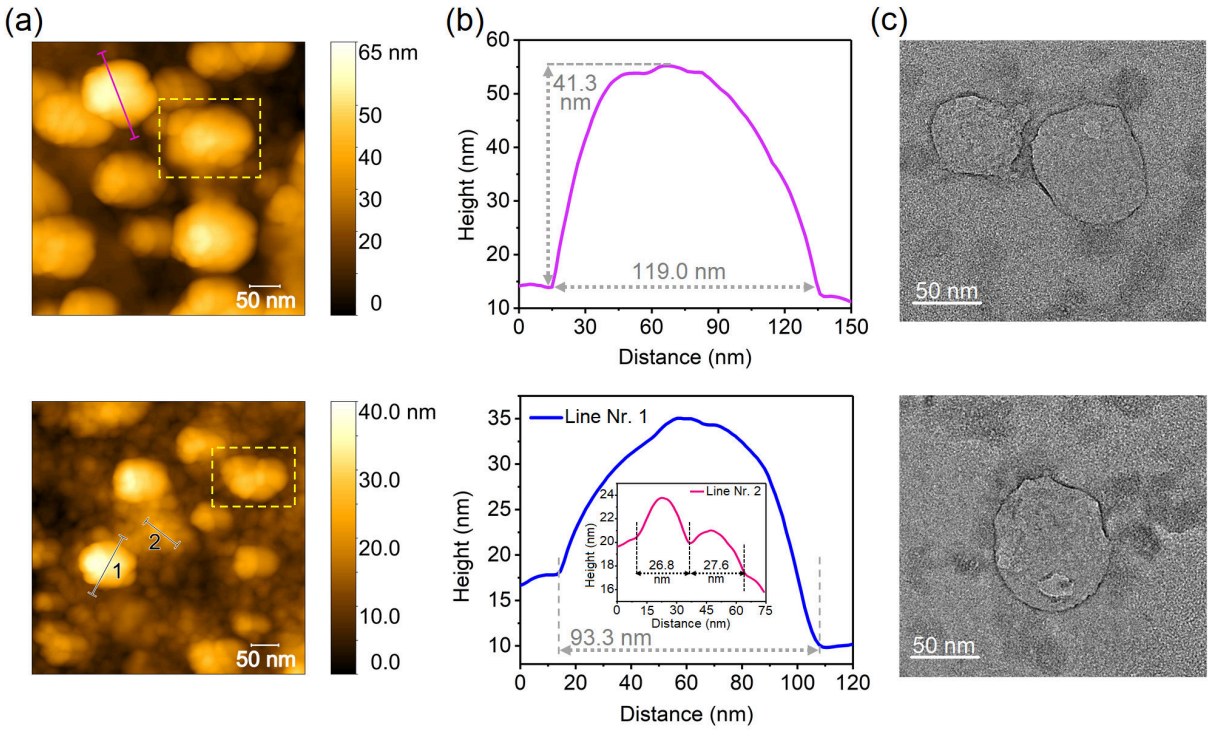

Figure 7: (a) AFM (0.5×0.5 μm^2) images of SARS-CoV-2 adsorbed on TiO_2(101) after UV treatment and (b) line scan profile measured along the particles in the AFM images. (c) TEM images of SARS-CoV-2 adsorbed on TiO_2(101) after UV treatment.

The role of Pd nanoparticles on SARS-CoV-2 adsorption on Pd/TiO_2(101)

To study the role of TiO_2 supported NPs on the adsorption behavior of SARS-CoV-2, Pd NPs were grown on the surface of TiO_2(101) using evaporation of Pd in UHV via physical

vapor deposition (see Methods section). Scanning tunneling microscopy (STM) (Figure 8 a) showed that the width of the Pd NPs is 3-4 nm (Figure 8 b). SARS-CoV-2 virus was loaded on the surface of the $Pd/TiO_2(101)$ and then inactivated by heating at 70 °C. AFM image of SARS-CoV-2 adsorbed on $Pd/TiO_2(101)$ exhibits a high number of particles with an average size around 80-120 nm that are related to the virus (Figure 8 c). Furthermore, larger particles were observed in the AFM image (Figure 8 d), which come from the interaction of the virus with Pd NPs resulting in the formation of complex structures. Similar behavior was reported for the Ag/TiO_2 catalyst, in which the interaction of the spike protein with Ag atoms and the subsequent formation of a SARS-CoV-2/Ag/TiO_2 complex enhanced the inactivation of the virus.[42] Wang et al. found that increasing the amount of Ag NPs on TiO_2 enhances the adsorption of SARS-CoV-2 in the liquid phase, although they did not study the surface of the solid catalyst and corresponding adsorption behavior of the virus.[42] Based on our observation and literature reports, we propose that the cause of higher adsorption and interaction of the virus with the $Pd/TiO_2(101)$ surface could be due to the binding of spike proteins with Pd NPs which enhances the adsorption efficiency compared to the bare TiO_2. Virus proteins contain carboxylic acid (–COOH), hydroxyl (–OH), amine ($–NH_2$), and carbonyl (C=O) functional groups.[41] Based on the surface charge of the substrate these functional groups can interact with the surface and enhance the adsorption ability of samples.[67–69] Cysteine ($C_3H_7NO_2S$) and asparagine ($C_4H_8N_2O_3$) are two abundant amino acids in the S-protein structure[42] with terminating carboxylic groups which are responsible for the connection of the virus to the surface of TiO_2. Moreover, the thiol group in the amino acid of the S-protein can interact with Pd NPs and generate complex structures (palladium cysteine thiolate). The interaction between the thiol group of the protein with the surface of Ag[70] and Au[71] metal NPs were observed earlier. So, the role of different functional groups in S-protein amino acids is important to understand the adsorption mechanism of virus on the surface of TiO_2.

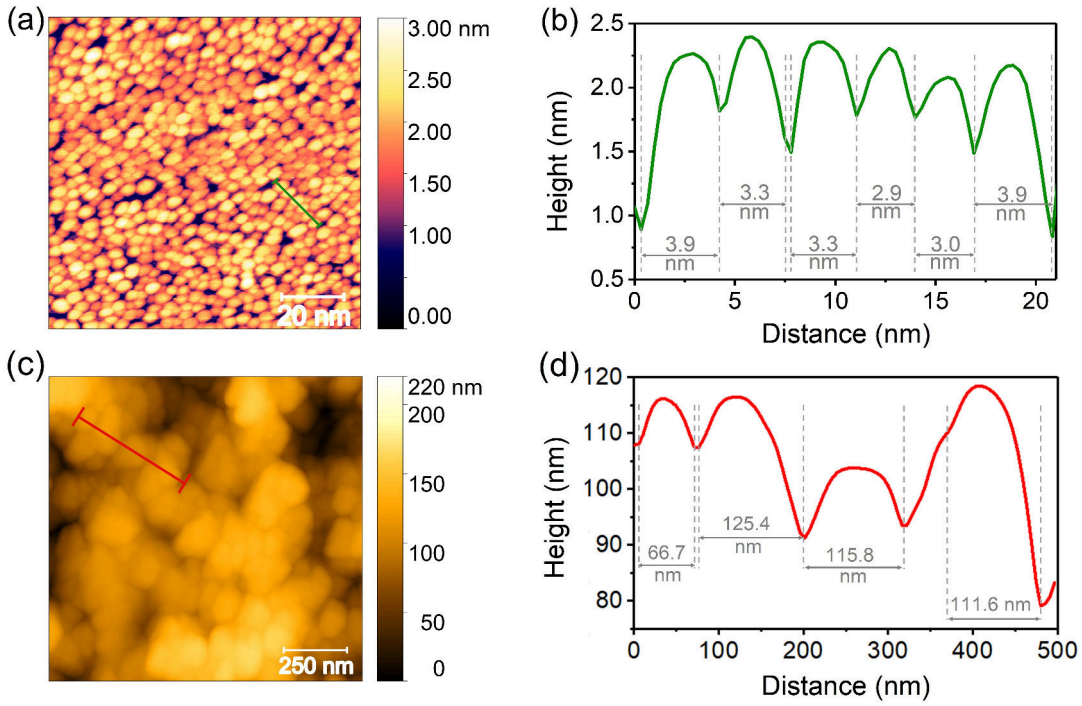

Figure 8: (a) STM image (0.1× 0.1 μm^2) of $Pd/TiO_2(101)$ at room temperature (Tunneling parameters: 1.5 V, 0.2 nA). (b) Line scan profile of marked particles in the STM image. (c) AFM (1.2× 1.2 μm^2) image of SARS-CoV-2 adsorbed on the surface of $Pd/TiO_2(101)$ catalyst after thermal treatment, and (d) line scan profile along the red line in the AFM image.

Proposed mechanism of adsorption and inactivation of SARS-CoV-2 on $TiO_2(101)$

The main step of virus adsorption on the surface of TiO_2 is related to the interaction of S-protein with the oxide surface, due to the high content of amino acids. Nitrogen and sulfur in cysteine and asparagine, with their paired electrons, can interact with Ti atoms which act as Lewis acid sites. Moreover, the surface oxygen atoms are Brönsted basic sites, and act as hydrogen (–H) bond acceptor.[49] So, functional groups such as $–NH_2$, –COOH, –SH, and –OH in the S-protein structure groups can interact with surface Ti and oxygen sites and enhance the adsorption of the virus particles. The charge of viral particles is dependent on the solution pH. The isoelectric point (IEP) of the virus is lower than 7.0.[39] Owing to the variety of proteins in virus structure and the large size of the virus, both negative and positive charges of surface functional groups exist in the virus structure between the range of pH=5.0-8.0 that

can enhance the adsorption efficiency of viruses on various surfaces.[41,72] Our results suggest that interaction of different functional groups in the virus proteins structure are responsible for adsorption of SARS-CoV-2 on the surface of TiO_2. During the thermal treatment virus proteins separate from the virus structure and adsorb on the surface of TiO_2(101). This changes of the virus structure under thermal treatment leads to the inactivation of virus on the surface. Three mechanisms can be responsible for SARS-CoV-2 inactivation under UV light irradiation on the surface of TiO_2(101): i) viral genome damage via absorption of UV irradiation by nucleic acid, ii) direct denaturation of viral proteins under UV light, and iii) photocatalytic oxidation of the viral particles. Utilizing TiO_2 as a photocatalyst enhances the disinfection efficiency of the surface owing to the oxidation/reduction of organic compounds in the viral proteins. Figure 9 shows the proposed mechanism of adsorption and inactivation of SARS-CoV-2 at the surface of TiO_2(101).

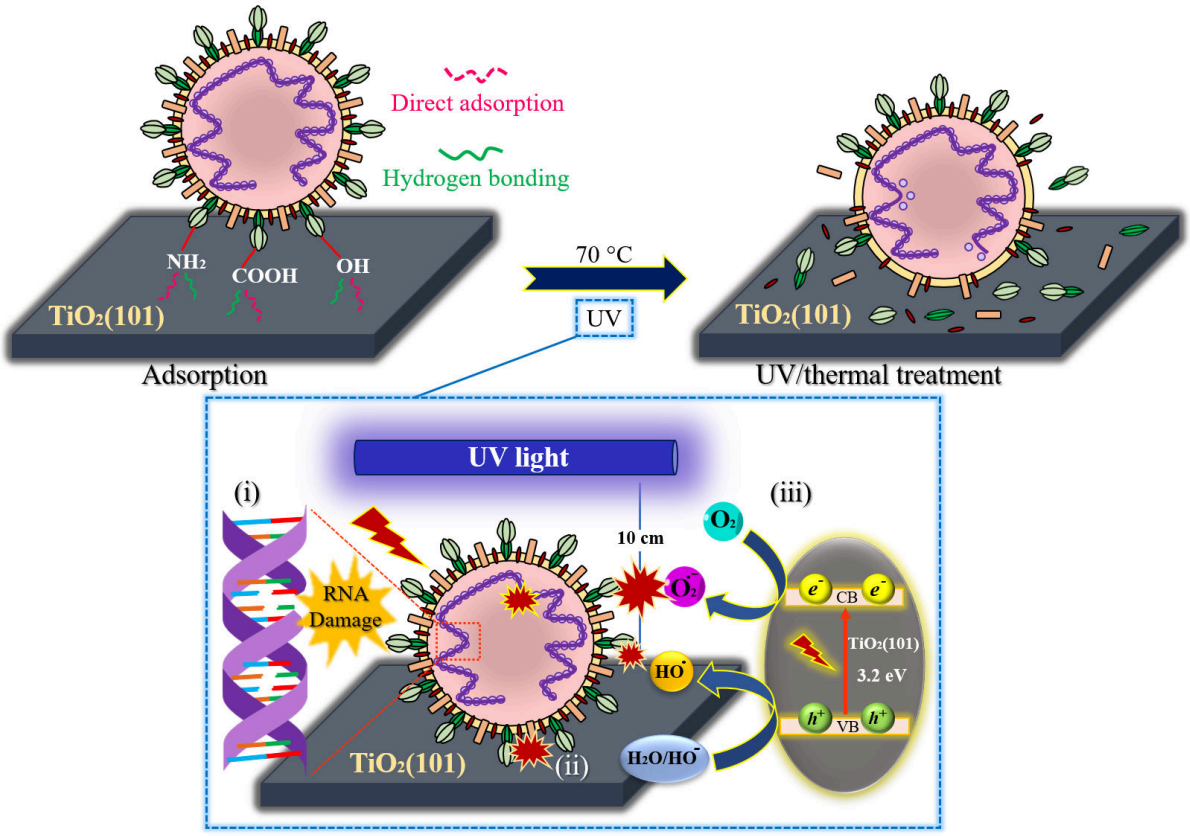

Figure 9: Proposed mechanism of SARS-CoV-2 adsorption, and the effect of thermal and UV treatments at the surface of $TiO_2(101)$. (i), (ii) and (iii) refer to the RNA damage, direct denaturation of S-protein and photocatalytic oxidation mechanism, respectively.

Conclusion

SARS-CoV-2 was adsorbed on the surface of the single crystalline anatase $TiO_2(101)$ and was studied after inactivation under thermal (at 70 °C), UV and ethanol treatments. Different microscopy techniques such as AFM, TEM and Florescence microscopy were used to investigate the adsorption, interaction and morphology of the virus/$TiO_2(101)$. Based on the AFM and TEM results, SARS-CoV-2 showed different interaction mechanisms under thermal, UV and ethanol treatments on the surface of titanium dioxide. In fact, following heat treatment of SARS-CoV-2 adsorbed on single crystal anatase surface, the virus proteins denature and dissociate from the virus structure, and subsequently readsorb on the catalyst surface. Thermal treatment changes the virus structure via the dissociation of proteins, while

ethanol dissolves the lipid bilayer resulting in the inactivation of the virus. Additionally, we performed XPS at the Ti 2p, C 1s, N 1s and O 1s core levels, which we combined with the theoretical XPS characterization of different models at the DFT level. The virus proteins lost their activity via close contact with the surface of TiO_2 and interaction of $–NH_2$ and –COOH groups at the surface of TiO_2, which was observed in the XP spectra. Moreover, the adsorbed virus showed aggregation behavior on the surface of the $Pd/TiO_2(101)$ catalyst. Interaction of functional groups of amino acids of the spike protein played vital role in the adhesion process, which highlighted the role of Pd NPs on virus adsorption. Plaque assay results demonstrated that SARS-CoV-2 particles adsorbed on the surface of $TiO_2(101)$ were efficiently inactivated by UV light within 30 min. The AFM and TEM results confirmed that UV irradiation has an effect on the adsorbed viral particles on the surface of $TiO_2(101)$ and changes the virus morphology, due to photocatalytic oxidation at the surface of TiO_2. The information obtained in this study will be vital for the development of air and surface cleaning materials from oxide catalysts/photocatalysts that are urgently required during the ongoing pandemic.

Experimental

Materials

The SARS-CoV-2 stock was supplied from Technical University of Munich (TUM). Sodium Pyruvate and fetal bovine serum (FBS) were supplied from Thermo Fischer Scientific GmbH (Dreieich, Germany). Glutamine, bovine serum albumin, Dulbecco's phosphate buffered saline (PBS), Bovine serum Albumin (BSA), and saponin were purchased from Sigma Aldrich. Non-essential amino acids (NEAA) and Dulbecco's Modified Eagle's Medium (DMEM) were purchased from Lonza (Lonza, Walkersville, MD, USA) and from Gibco (New York, USA). Penicillin/Streptomycin was obtained from Gibco (New York, USA).

Preparation of SARS-CoV-2

The SARS-CoV-2 isolate hCoV-19/Germany/BAV-PL-virotum-nacq/2020 (GISAID accession ID: EPIISL582134) was derived from a nasopharyngeal swap of a 2 years old boy. The SARS-CoV-2 stock was propagated in the biosafety level 3 (BSL3) laboratory at the institute of Virology, TUM. VeroE6 cells at a confluency of about 60% were inculated with 1.0 mL of the isolated virus and 9.0 mL of DMEM containing 5.0% FBS, L-Glutamine (2.0 mM), Penicilin /Streptomycin (50 U mL^{-1}), 1.0% non-essential amino acids, and sodium pyruvate (1.0 mM), at 37.0 °C. 24- and 28-hours post-inoculation, the supernatant was harvested and centrifuged for 10 min at 300xg and stored at -80 °C.

Preparation of $Pd/TiO_2(101)$ catalyst

The anatase $TiO_2(101)$ single crystal (5 mm x 5 mm x 2 mm, Surface net Ltd.) was prepared by repeated 1 keV Ar^+ ion bombardment and 850 K anneal cycles in a backpressure of 1×10^{-6} mbar O_2, until XPS showed the surface to be free of contamination. The Pd nanoparticles were deposited at room temperature on the surface of vacuum prepared titanium dioxide (as outlined above) by means of Pd metal vapor deposition in an UHV chamber, with a base pressure of 1×10^{-10} mbar.

Adsorption and inactivation of SARS-CoV-2 on the surface of $TiO_2(101)$

To study the adsorption behavior of SARS-CoV-2, 10.0 µL SARS-CoV-2 stock containing 10.000 plaque forming units (PFU) (10^6 PFU/mL) was loaded on the center of catalyst crystal structure so that the whole catalyst surface was covered. To inactivate the adsorbed virus on the surface of $TiO_2(101)$ and $Pd/TiO_2(101)$ by thermal inactivation method, the samples were placed in an incubator and heated to 70 °C for 30 min. A similar method was applied for coating the CCM (without SARS-CoV-2) on the surface of $TiO_2(101)$. To compare the effect of different inactivation methods on adsorbed virus structure, ethanol treatment was

also investigated on adsorbed SARS-CoV-2 particles. Additionally, UV irradiation (Wavelength: 265 nm; 30 min irradiation time; 10 cm distance to the light source) was investigated as an inactivation method. For the control experiment, the system was kept in the dark for 30 min. All experiments were performed in a biosafety level (BSL)-3 laboratory. Plaque assay was performed as described in Stukalov, A. et al. 2021.[73] to determine remaining viral titers in irradiated samples and check for successful inactivation of infectious virus particles. After UV treatment, no infectious virus was detected contrary to the dark condition. By using these methods, we were able to transfer the sample to lower safety laboratories for the characterization.

Characterization methods

Fluorescence microscopy Fluorescence microscopy was used to prove binding of SARS-CoV viral particles to TiO_2 crystals via detection with rabbit anti-SARS-CoV-2 nucleocapsid primary antibodies and anti-rabbit secondary antibodies conjugated to the fluorescent dye Alexa568. Since the SARS-CoV-2 adsorbed on TiO_2(101) was heated at 70 °C as heating treatment, the CCM on TiO_2(101) was prepared as reference sample under the same condition. The surface of TiO_2(101) was covered by CCM and the sample was dried in an incubator at 70 °C. To reduce non-specific antibody binding, the sample was covered with blocking solution (PBS supplemented with Saponin (0.25%) and Bovine serum Albumin (BSA, 3.0%). After 30 min, the sample was washed three times with PBS. Then, 20 µL of blocking solution containing 1:200 diluted primary antibody (anti - SARS-CoV-2 nucleocapsid antibody produced in rabbit, Thermo Fisher Scientific), was added on the top of the sample. After incubation time (1 h), the sample was washed with PBS to remove unbound antibody and then blocking solution containing 1:500 fluorescent-dye conjugated secondary antibody (anti-rabbit antibody conjugated with Alexa568, Thermo Fisher Scientific) was added. After an incubation (30 min) and washing (three times by PBS), the samples were examined with a fluorescence microscope (Leica DMi8 equipped with a 20x

NA 0.4 air objective, a Leica DFC9000 GT sCMOS camera, and a Lumencore Sola SE FISH 365 LED light source).

Atomic force microscopy (AFM) AFM was used for investigating the interaction of SARS-CoV-2 with the surface of the samples. AFM imaging was performed using a CP-II instrument from Digital Instruments at DESY Nanolab.[66] The AFM images were recorded under intermittent (tapping) mode, wiht different scan sizes (2.5× 2.5 μm^2 and 5.0× 5.0 μm^2) and 0.996 Hz scan rate.

Transmission electron microscopy (TEM) To investigate the morphology of adsorbed virus on TiO_2 by TEM, some coating of three substrates that inactivated by ethanol, thermal and UV treatments was scrapped with a blade. Then, the blades were rinsed with ethanol and were loaded on the carbon grids. The TEM images of theses samples were recorded on a FEI Talos F200X (typo Thermo Fisher Scientific, USA) at 200 kV.

X-ray photoelectron spectroscopy HAXPES data were collected at beamline P22 at PETRA III at the Deutsches Electron Synchrotron DESY[74] in Hamburg, Germany. A photon energy of 3.4 keV was used for all experiments, with the energy selected using a Si (111) double crystal monochromator and a Si (220) post-monochromator. All measurements were conducted in grazing incidence geometry (9°). A Phoibos 225HV analyzer (SPECS, Berlin, Germany) was used with the small area lens mode and a slit size of 3 mm. Spectra were collected using a pass energy of 50 eV, and a total energy resolution of about 300 meV. The XPS measurements for adsorbed CCM on TiO_2(101) were carried out using XPS system in the DESY Nanolab,[66] at the Centre for X-ray and Nano Science, DESY. The X-ray source employed was Al Kα at 1.4 keV and a Phoibos 150 hemispherical energy analyzer with a base pressure of 1.2×10^{-10} mbar. The core-level spectra for the CCM adsorbed on TiO_2 are normalized to the intensity of Ti $2p_{3/2}$ peaks of clean surface of TiO_2 while the core-level spectra for the SARS-CoV-2 adsorbed on TiO_2 are normalized to the corresponding Ti $2p_{3/2}$

peaks. All XPS spectra were fitted by CasaXPS software,[75] while the Shirley background and Gaussian curves were utilized.

Scanning tunneling microscopy (STM) The STM measurements were performed in a Scienta Omicron VT SPM with a base pressure of 4×10^{-11} mbar in constant current mode using a tungsten tip at DESY Nanolab.[66] STM and AFM images processing was done using the Gwyddion software package.[76]

Computational methods

All the calculations have been performed within the density functional theory framework, through the QUANTUM Espresso suite,[77–79] including the PBE exchange-correlation functional with a plane-waves basis set size of 52 and 575 Ry for the ground state wave function and charge density, respectively. The TiO_2 anatase (101) surface has been modeled through a slab made of three triatomic-layers with a 4×1 supercell including at least 11 Å along the non-periodic z direction. The lowermost layer has been kept fixed to the positions optimized in the bulk structure (with lattice parameters a=3.790 Å and c=10.325 Å) while the others have been left free to relax. The wave function has been expanded onto a shifted 2×2×1 grid of points in reciprocal space, generated by the Monkhorst-Pack algorithm. Dispersion interactions have been accounted for by the inclusion of an additional charge-dependent term to the forces through the Grimme-D3 correction.[80] The XP spectra have been simulated at the C K-edge through the ΔSCF method,[81] for which an additional pseudopotential, generated with a missing 1s electron in the core states, is placed at every inequivalent core-excited atom in the supercell. Such a pseudopotential requires an enlarged plane-waves basis set, up to 74 and 575 Ry. In addition, since we relied on pseudopotentials, we couldn't directly calculate the absolute BE but rather its relative change energy with respect to a selected reference, i.e. the core level shift (CLS). To compare the CLS calculated for inequivalent atoms in different models, we included in each supercell a common reference, namely an

ethylene (C_2H_4) molecule, in each supercell at more than 15 Å from the surface, minimizing its interaction with the slab. A similar approach has been successfully applied in previous works.[82–85] Finally, the simulated XP spectra have been constructed through the convolution of the calculated CLS with Gaussian profiles, with broadening σ=0.17 eV.

Acknowledgement

This study was supported by the initiative and networking fund of the Helmholtz Association of German Research Centers under the CORAERO Project (KA1-Co-06). The authors acknowledge DESY (Hamburg, Germany), a member of the Helmholtz Association HGF, for the provision of experimental facilities. Parts of this research were carried out at PETRA III using beamline P22. Funding for the HAXPES instrument by the Federal Ministry of Education and Research (BMBF) under framework program ErUM is gratefully acknowledged. MK and HN thank Wolfgang Hammerschmidt for helpful discussion and information. CDV acknowledges support from the European Research Council (ERC) under the European Union's HORIZON2020 research and innovation programme (ERC Grant Agreement No [647020]).

Supporting Information Available

The following files are available free of charge.

- S1: Fluorescence images of CCM (a), and SARS-CoV-2 (b) adsorbed on TiO_2(101) after thermal treatment.
- S2: X-ray absorption at C 1*s* edge binding energies (BE): comparison between experimental and calculated values. The latter are reported as differences from an arbitrary reference, which in this case has been set to the component with the lowest BE.

References

(1) Stanborough, T.; Given, F. M.; Koch, B.; Sheen, C. R.; Stowers-Hull, A. B.; Waterland, M. R.; Crittenden, D. L. Optical detection of CoV-SARS-2 viral proteins to sub-picomolar concentrations. *ACS omega* **2021**, *6*, 6404–6413.

(2) Yadav, R.; Chaudhary, J. K.; Jain, N.; Chaudhary, P. K.; Khanra, S.; Dhamija, P.; Sharma, A.; Kumar, A.; Handu, S. Role of structural and non-structural proteins and therapeutic targets of SARS-CoV-2 for COVID-19. *Cells* **2021**, *10*, 821.

(3) Seah, I.; Su, X.; Lingam, G. Revisiting the dangers of the coronavirus in the ophthalmology practice. *Eye* **2020**, *34*, 1155–1157.

(4) Turoňová, B.; Sikora, M.; Schürmann, C.; Hagen, W. J.; Welsch, S.; Blanc, F. E.; von Bülow, S.; Gecht, M.; Bagola, K.; Hörner, C., et al. In situ structural analysis of SARS-CoV-2 spike reveals flexibility mediated by three hinges. *Science* **2020**, *370*, 203–208.

(5) Lorenzo, R.; Defelipe, L. A.; Aliperti, L.; Niebling, S.; Custódio, T. F.; Löw, C.; Schwarz, J. J.; Remans, K.; Craig, P. O.; Otero, L. H., et al. Deamidation drives molecular aging of the SARS-CoV-2 spike protein receptor-binding motif. *Journal of Biological Chemistry* **2021**, *297*.

(6) Papageorgiou, A. C.; Mohsin, I. The SARS-CoV-2 spike glycoprotein as a drug and vaccine target: structural insights into its complexes with ACE2 and antibodies. *Cells* **2020**, *9*, 2343.

(7) Pal, M.; Berhanu, G.; Desalegn, C.; Kandi, V. Severe acute respiratory syndrome coronavirus-2 (SARS-CoV-2): an update. *Cureus* **2020**, *12*.

(8) Chen, Y.-C.; Huang, L.-M.; Chan, C.-C.; Su, C.-P.; Chang, S.-C.; Chang, Y.-Y.;

Chen, M.-L.; Hung, C.-C.; Chen, W.-J.; Lin, F.-Y., et al. SARS in hospital emergency room. *Emerging infectious diseases* **2004**, *10*, 782.

(9) Ortega, K., et al. PHB. SARS-CoV-2 and dentistry. *Clin Oral Investig* **2020**, 1–2.

(10) Ong, S. W. X.; Tan, Y. K.; Chia, P. Y.; Lee, T. H.; Ng, O. T.; Wong, M. S. Y.; Marimuthu, K. Air, surface environmental, and personal protective equipment contamination by severe acute respiratory syndrome coronavirus 2 (SARS-CoV-2) from a symptomatic patient. *Jama* **2020**, *323*, 1610–1612.

(11) Celik, U.; Celik, K.; Celik, S.; Abayli, H.; Sahna, K. C.; Tonbak, Ş.; Toraman, Z. A.; Oral, A. Interpretation of SARS-CoV-2 behaviour on different substrates and denaturation of virions using ethanol: an atomic force microscopy study. *Rsc Advances* **2020**, *10*, 44079–44086.

(12) Lyonnais, S.; Hénaut, M.; Neyret, A.; Merida, P.; Cazevieille, C.; Gros, N.; Chable-Bessia, C.; Muriaux, D. Atomic force microscopy analysis of native infectious and inactivated SARS-CoV-2 virions. *Scientific reports* **2021**, *11*, 1–7.

(13) Patterson, E. I.; Prince, T.; Anderson, E. R.; Casas-Sanchez, A.; Smith, S. L.; Cansado-Utrilla, C.; Solomon, T.; Griffiths, M. J.; Acosta-Serrano, Á.; Turtle, L., et al. Methods of inactivation of SARS-CoV-2 for downstream biological assays. *The Journal of infectious diseases* **2020**, *222*, 1462–1467.

(14) Barclay, L.; Park, G.; Vega, E.; Hall, A.; Parashar, U.; Vinjé, J.; Lopman, B. Infection control for norovirus. *Clinical microbiology and infection* **2014**, *20*, 731–740.

(15) Storm, N.; McKay, L. G.; Downs, S. N.; Johnson, R. I.; Birru, D.; de Samber, M.; Willaert, W.; Cennini, G.; Griffiths, A. Rapid and complete inactivation of SARS-CoV-2 by ultraviolet-C irradiation. *Scientific Reports* **2020**, *10*, 1–5.

(16) Pastorino, B.; Touret, F.; Gilles, M.; de Lamballerie, X.; Charrel, R. N. Heat inactivation of different types of SARS-CoV-2 samples: what protocols for biosafety, molecular detection and serological diagnostics? *Viruses* **2020**, *12*, 735.

(17) Singh, L.; Kruger, H. G.; Maguire, G. E.; Govender, T.; Parboosing, R. The role of nanotechnology in the treatment of viral infections. *Therapeutic advances in infectious disease* **2017**, *4*, 105–131.

(18) Chu, C.; Ryberg, E. C.; Loeb, S. K.; Suh, M.-J.; Kim, J.-H. Water disinfection in rural areas demands unconventional solar technologies. *Accounts of Chemical Research* **2019**, *52*, 1187–1195.

(19) Nakano, R.; Yamaguchi, A.; Sunada, K.; Nagai, T.; Nakano, A.; Suzuki, Y.; Yano, H.; Ishiguro, H.; Miyauchi, M. Inactivation of various variant types of SARS-CoV-2 by indoor-light-sensitive TiO2-based photocatalyst. *Scientific reports* **2022**, *12*, 1–10.

(20) Kamegawa, T.; Shimizu, Y.; Yamashita, H. Superhydrophobic surfaces with photocatalytic self-cleaning properties by nanocomposite coating of TiO_2 and polytetrafluoroethylene. *Advanced Materials* **2012**, *24*, 3697–3700.

(21) Tung, W. S.; Daoud, W. A. Self-cleaning fibers via nanotechnology: a virtual reality. *Journal of Materials Chemistry* **2011**, *21*, 7858–7869.

(22) Diebold, U. The surface science of titanium dioxide. *Surface science reports* **2003**, *48*, 53–229.

(23) Wagstaffe, M.; Wenthaus, L.; Dominguez-Castro, A.; Chung, S.; Lana Semione, G. D.; Palutke, S.; Mercurio, G.; Dziarzhytski, S.; Redlin, H.; Klemke, N., et al. Ultrafast real-time dynamics of CO oxidation over an oxide photocatalyst. *ACS catalysis* **2020**, *10*, 13650–13658.

(24) Park, H.; Bentria, E. T.; Rtimi, S.; Arredouani, A.; Bensmail, H.; El-Mellouhi, F. Accelerating the Design of Photocatalytic Surfaces for Antimicrobial Application: Machine Learning Based on a Sparse Dataset. *Catalysts* **2021**, *11*, 1001.

(25) Thomas, N.; Dionysiou, D. D.; Pillai, S. C. Heterogeneous Fenton catalysts: A review of recent advances. *Journal of Hazardous Materials* **2021**, *404*, 124082.

(26) Li, R.; Cui, L.; Chen, M.; Huang, Y. Nanomaterials for airborne virus inactivation: a short review. *Aerosol Science and Engineering* **2021**, *5*, 1–11.

(27) Habibi-Yangjeh, A.; Asadzadeh-Khaneghah, S.; Feizpoor, S.; Rouhi, A. Review on heterogeneous photocatalytic disinfection of waterborne, airborne, and foodborne viruses: Can we win against pathogenic viruses? *Journal of Colloid and Interface Science* **2020**, *580*, 503–514.

(28) Fujishima, F. TiO_2 photocatalysis fundamentals and applications. *A Revolution in cleaning technology* **1999**, 14–21.

(29) Hashimoto, K.; Irie, H.; Fujishima, A. TiO_2 photocatalysis: a historical overview and future prospects. *Japanese journal of applied physics* **2005**, *44*, 8269.

(30) Fujishima, A.; Zhang, X.; Tryk, D. A. TiO_2 photocatalysis and related surface phenomena. *Surface science reports* **2008**, *63*, 515–582.

(31) Matsuura, R.; Lo, C.-W.; Wada, S.; Somei, J.; Ochiai, H.; Murakami, T.; Saito, N.; Ogawa, T.; Shinjo, A.; Benno, Y., et al. SARS-CoV-2 disinfection of air and surface contamination by tio2 photocatalyst-mediated damage to viral morphology, RNA, and protein. *Viruses* **2021**, *13*, 942.

(32) Kampf, G.; Todt, D.; Pfaender, S.; Steinmann, E. Persistence of coronaviruses on inanimate surfaces and their inactivation with biocidal agents. *Journal of hospital infection* **2020**, *104*, 246–251.

(33) Imani, S. M.; Ladouceur, L.; Marshall, T.; Maclachlan, R.; Soleymani, L.; Didar, T. F. Antimicrobial nanomaterials and coatings: Current mechanisms and future perspectives to control the spread of viruses including SARS-CoV-2. *ACS nano* **2020**, *14*, 12341–12369.

(34) Djellabi, R.; Basilico, N.; Delbue, S.; D'Alessandro, S.; Parapini, S.; Cerrato, G.; Laurenti, E.; Falletta, E.; Bianchi, C. L. Oxidative inactivation of SARS-CoV-2 on photoactive AgNPs@ TiO_2 ceramic tiles. *International Journal of Molecular Sciences* **2021**, *22*, 8836.

(35) Jiang, D.; Ni, D.; Rosenkrans, Z. T.; Huang, P.; Yan, X.; Cai, W. Nanozyme: new horizons for responsive biomedical applications. *Chemical Society Reviews* **2019**, *48*, 3683–3704.

(36) Dubois, L. H.; Zegarski, B. R.; Nuzzo, R. G. Fundamental studies of microscopic wetting on organic surfaces. 2. Interaction of secondary adsorbates with chemically textured organic monolayers. *Journal of the American chemical Society* **1990**, *112*, 570–579.

(37) Elechiguerra, J. L.; Burt, J. L.; Morones, J. R.; Camacho-Bragado, A.; Gao, X.; Lara, H. H.; Yacaman, M. J. Interaction of silver nanoparticles with HIV-1. *Journal of nanobiotechnology* **2005**, *3*, 1–10.

(38) Tabish, T. A.; Hamblin, M. R. Multivalent nanomedicines to treat COVID-19: A slow train coming. *Nano Today* **2020**, *35*, 100962.

(39) Michen, B.; Graule, T. Isoelectric points of viruses. *Journal of applied microbiology* **2010**, *109*, 388–397.

(40) Castaño, N.; Cordts, S. C.; Kurosu Jalil, M.; Zhang, K. S.; Koppaka, S.; Bick, A. D.; Paul, R.; Tang, S. K. Fomite transmission, physicochemical origin of virus–surface interactions, and disinfection strategies for enveloped viruses with applications to SARS-CoV-2. *ACS omega* **2021**, *6*, 6509–6527.

(41) Joonaki, E.; Hassanpouryouzband, A.; Heldt, C. L.; Areo, O. Surface chemistry can unlock drivers of surface stability of SARS-CoV-2 in a variety of environmental conditions. *Chem* **2020**, *6*, 2135–2146.

(42) Wang, D.; Zhang, B.; Ding, H.; Liu, D.; Xiang, J.; Gao, X. J.; Chen, X.; Li, Z.; Yang, L.; Duan, H., et al. TiO_2 supported single Ag atoms nanozyme for elimination of SARS-CoV2. *Nano today* **2021**, *40*, 101243.

(43) Miyauchi, M.; Sunada, K.; Hashimoto, K. Antiviral effect of visible light-sensitive Cu_xO/TiO_2 photocatalyst. *Catalysts* **2020**, *10*, 1093.

(44) Lu, Y.; Guan, S.; Hao, L.; Yoshida, H.; Nakada, S.; Takizawa, T.; Itoi, T. Inactivation of SARS-CoV-2 and photocatalytic degradation by TiO2 photocatalyst coatings. *Scientific reports* **2022**, *12*, 1–8.

(45) Jiang, H. B.; Cuan, Q.; Wen, C. Z.; Xing, J.; Wu, D.; Gong, X.-Q.; Li, C.; Yang, H. G. Anatase TiO_2 crystals with exposed high-index facets. *Angewandte Chemie* **2011**, *123*, 3848–3852.

(46) Walls, A. C.; Park, Y.-J.; Tortorici, M. A.; Wall, A.; McGuire, A. T.; Veesler, D. Structure, function, and antigenicity of the SARS-CoV-2 spike glycoprotein. *Cell* **2020**, *181*, 281–292.

(47) Rath, S. L.; Kumar, K. Investigation of the effect of temperature on the structure of SARS-CoV-2 Spike Protein by Molecular Dynamics Simulations. *Frontiers in molecular biosciences* **2020**, 297.

(48) Golin, A. P.; Choi, D.; Ghahary, A. Hand sanitizers: A review of ingredients, mechanisms of action, modes of delivery, and efficacy against coronaviruses. *American journal of infection control* **2020**, *48*, 1062–1067.

(49) Pantaleone, S.; Rimola, A.; Sodupe, M. Canonical, deprotonated, or zwitterionic? A computational study on amino acid interaction with the TiO2 (101) anatase surface. *The Journal of Physical Chemistry C* **2017**, *121*, 14156–14165.

(50) Zubavichus, Y.; Fuchs, O.; Weinhardt, L.; Heske, C.; Umbach, E.; Denlinger, J. D.; Grunze, M. Soft X-ray-induced decomposition of amino acids: an XPS, mass spectrometry, and NEXAFS study. *Radiation Research* **2004**, *161*, 346–358.

(51) Liu, L.; Li, K.; Chen, X.; Liang, X.; Zheng, Y.; Li, L. Amino acid adsorption on anatase (101) surface at vacuum and aqueous solution: a density functional study. *Journal of Molecular Modeling* **2018**, *24*, 1–9.

(52) Hu, W.; Liu, Y.; Withers, R. L.; Frankcombe, T. J.; Norén, L.; Snashall, A.; Kitchin, M.; Smith, P.; Gong, B.; Chen, H., et al. Electron-pinned defect-dipoles for high-performance colossal permittivity materials. *Nature materials* **2013**, *12*, 821–826.

(53) Wagstaffe, M.; Noei, H.; Stierle, A. Elucidating the defect-induced changes in the photocatalytic activity of TiO_2. *The Journal of Physical Chemistry C* **2020**, *124*, 12539–12547.

(54) Liu, H.; Zhang, Q.; Hu, H.; Li, A.; Yao, H. Influence of residual moisture on deep dewatered sludge pyrolysis. *International journal of hydrogen energy* **2014**, *39*, 1253–1261.

(55) Sousa, S.; Moradas-Ferreira, P.; Barbosa, M. TiO_2 type influences fibronectin adsorption. *Journal of Materials Science: Materials in Medicine* **2005**, *16*, 1173–1178.

(56) Wang, X.; Wang, J.; Yang, Z.; Leng, Y.; Sun, H.; Huang, N. Structural characterization and mechanical properties of functionalized pulsed-plasma polymerized allylamine film. *Surface and Coatings Technology* **2010**, *204*, 3047–3052.

(57) Wagstaffe, M.; Hussain, H.; Taylor, M.; Murphy, M.; Silikas, N.; Thomas, A. G. Interaction of a tripeptide with titania surfaces: RGD adsorption on rutile TiO_2 (110) and model dental implant surfaces. *Materials Science and Engineering: C* **2019**, *105*, 110030.

(58) Yang, D.-Q.; Hennequin, B.; Sacher, E. XPS demonstration of π- π interaction between benzyl mercaptan and multiwalled carbon nanotubes and their use in the adhesion of Pt nanoparticles. *Chemistry of Materials* **2006**, *18*, 5033–5038.

(59) Stewart-Ornstein, J.; Hitchcock, A. P.; Hernández Cruz, D.; Henklein, P.; Overhage, J.; Hilpert, K.; Hale, J. D.; Hancock, R. E. Using intrinsic X-ray absorption spectral differences to identify and map peptides and proteins. *The Journal of Physical Chemistry B* **2007**, *111*, 7691–7699.

(60) Sliman, H.; Dong, X.; Zhao, T. Functionalization of polyethylene terephthalate knitted fabric with cowpea protein and biopolymer complex: Applications for enhancing wettability and UV-Protection properties. *Journal of Colloid and Interface Science* **2020**, *565*, 360–367.

(61) Jain, M.; Unnikrishnan, R.; Martin, V.; Mehta, A.; Bhatnagar, A. An ESCA study of the effectiveness of antiwear and extreme-pressure additives based on substituted phosphorodithioate derivatives, and a comparison with ZDDP. *Tribotest* **2001**, *8*, 107–122.

(62) Raeiszadeh, M.; Adeli, B. A critical review on ultraviolet disinfection systems against COVID-19 outbreak: applicability, validation, and safety considerations. *Acs Photonics* **2020**, *7*, 2941–2951.

(63) Uppal, T.; Reganti, S.; Martin, E.; Verma, S. C. Surface Inactivation of Human Coronavirus by MACOMA™ UVA-TiO2 Coupled Photocatalytic Disinfection System. *Catalysts* **2022**, *12*, 690.

(64) Lo, C.-W.; Matsuura, R.; Iimura, K.; Wada, S.; Shinjo, A.; Benno, Y.; Nakagawa, M.; Takei, M.; Aida, Y. UVC disinfects SARS-CoV-2 by induction of viral genome damage without apparent effects on viral morphology and proteins. *Scientific reports* **2021**, *11*, 1–11.

(65) Beck, S. E.; Rodriguez, R. A.; Linden, K. G.; Hargy, T. M.; Larason, T. C.; Wright, H. B. Wavelength dependent UV inactivation and DNA damage of adenovirus as measured by cell culture infectivity and long range quantitative PCR. *Environmental science & technology* **2014**, *48*, 591–598.

(66) Stierle, A.; Keller, T. F.; Noei, H.; Vonk, V.; Roehlsberger, R. Desy nanolab. *Journal of large-scale research facilities JLSRF* **2016**, *2*, 76.

(67) Dika, C.; Ly-Chatain, M.; Francius, G.; Duval, J.; Gantzer, C. Non-DLVO adhesion of F-specific RNA bacteriophages to abiotic surfaces: importance of surface roughness, hydrophobic and electrostatic interactions. *Colloids and Surfaces A: Physicochemical and Engineering Aspects* **2013**, *435*, 178–187.

(68) Xie, L.; Liu, F.; Liu, J.; Zeng, H. A nanomechanical study on deciphering the stickiness of SARS-CoV-2 on inanimate surfaces. *ACS applied materials & interfaces* **2020**, *12*, 58360–58368.

(69) Ding, Z.; Wang, H.; Feng, Z.; Sun, M. Synthesis of dual-phase Ti_3O_5/Ti_4O_7 nanofibers for efficient adsorption of SARS-CoV-2. *Materials Letters* **2021**, *300*, 130167.

(70) Jiang, H. S.; Zhang, Y.; Lu, Z. W.; Lebrun, R.; Gontero, B.; Li, W. Interaction between silver nanoparticles and two dehydrogenases: Role of thiol groups. *Small* **2019**, *15*, 1900860.

(71) Yüce, M.; Kurt, H. How to make nanobiosensors: surface modification and characterisation of nanomaterials for biosensing applications. *RSC advances* **2017**, *7*, 49386–49403.